Radiative mixed convective flow induced by hybrid nanofluid over a porous vertical cylinder in a porous media with irregular heat sink/source

Umair Khan [a,b], Aurang Zaib [c], Anuar Ishak [a], El-Sayed M. Sherif [d], Iskandar Waini [e], Yu-Ming Chu [f,g,*], Ioan Pop [h]

[a] *Department of Mathematical Sciences, Faculty of Science and Technology, Universiti Kebangsaan Malaysia, UKM Bangi, 43600, Selangor, Malaysia*
[b] *Department of Mathematics and Social Sciences, Sukkur IBA University, Sukkur, 65200, Sindh, Pakistan*
[c] *Department of Mathematical Sciences, Federal Urdu University of Arts, Science & Technology, Gulshan-e-Iqbal, Karachi, 75300, Pakistan*
[d] *Mechanical Engineering Department, College of Engineering, King Saud University, Riyadh, 11423, Saudi Arabia*
[e] *Fakulti Teknologi Kejuruteraan Mekanikal dan Pembuatan, Universiti Teknikal Malaysia Melaka, Hang Tuah Jaya, 76100, Durian Tunggal, Melaka, Malaysia*
[f] *Institute for Advanced Study Honoring Chen Jian Gong, Hangzhou Normal University, Hangzhou, 311121, PR China*
[g] *Department of Mathematics, Huzhou University, Huzhou, 313000, PR China*
[h] *Department of Mathematics, Babeş-Bolyai University, 400084, Cluj-Napoca, Romania*

ARTICLE INFO

ABSTRACT

Purpose: Hybrid nanofluids have higher mechanical resistance, thermal conductivity, chemical stability, and physical strength when compared to normal nanofluids. Our approach in the current paper is to present a novel exploration comprising radiative mixed convection flow of hybrid nanofluids with irregular heat source/sink effect through a porous vertical cylinder immersed in a porous media. Both opposing and assisting flows are discussed.
Methodology: The transmuted similarity ODEs are numerically worked out utilizing the assist of the bvp4c package in MATLAB for different values of physical parameters. The hybrid nanofluids contain a couple of nanoparticles namely aluminum and copper particles with water as base fluid.
Findings: It was observed that fundamental similarity equations disclose double solutions (first and second branches) for buoyancy assisting and opposing flows. The drag force is enhanced due to the radiation as well as curvature parameters. In addition, the velocity declines due to heat source/sink and radiation parameter.
Originality/value: The writers agree that all numerical outcomes are novel and have not previously been published for the current problem.

1. Introduction

Heat transfer enhancement is important in the engineering and industrial sectors. Regular fluids like ethylene glycol and water are used as cooling (operating) liquids in machine operations. Even though the use of regular fluids can reduce operating costs, but the increment in heat transfer is ineffective due to their low thermal conductivity. Thus, nanofluids are proposed and validated through

numerical and experimental studies to get the best thermal productivity. The exploration of heat transfer liquid by Choi and Eastman [1] has endorsed numerous investigators to prolong the inquests and develop innovative nanofluids with comprehensively superior thermal conductivities. Hayat et al. [2] inspected the radiation effect and slip condition mechanism in the existence of water-based Ag–CuO nanofluids. Khan et al. [3] mentioned the fluid flow of nanofluids induced by a model of tangent hyperbolic imposing on a stretchable cylinder in the stagnation region. The behavior of temperature on the time-dependent flow conveying water-based nanofluid via moving parallel plates was Shahriari et al. [4]. They have shown that the viscous dissipative ratio of TiO_2 nanoparticles is higher compared to other nanoparticles. Maghsoudi et al. [5] examined the impact of thermal radiation and magnetic field on the free convective flow induced by non-Newtonian nanofluid between two-infinite flat vertical plates and utilized the Galerkin technique to find the solution. Gorgani et al. [6] utilized the artificial neural network to discuss the behavior of time-dependent squeezing flow induced by nanofluid among a couple of parallel plates. Dede et al. [7] showed that the hot body emitter can be selected directly to transfer the heat towards a cold body by improving the design of the emitter body's anisotropic thermal conductivity and surface emissivity. Xu et al. [8] presented a novel technique for manipulating thermal fields that employs a reconfigurable two-phase thermal meta-material made up of transparent liquid and manageable micro magnetic particles. Recently, the flow of nanofluids over an extending surface in the existence of various factors was inspected by several researchers [9–13]. More recently, Swain and Mahanthesh [14] studied the nanoparticles aggregation effects on the three-dimensional radiative flow induced by water-based titanium nanofluid past an elongated exponential surface with Joule heating and heat sink/source. The impact of an inclined magnetic and exponentially based heat source effects on the flow past a shrinking/elongating sheet were explored by Swain et al. [15]. They have observed that the velocity of fluid decelerates while the temperature accelerates due to magnetic influence. Swain et al. [16] inspected the impact of the irregular magnetic effect on the flow of water-based Fe_3O_4/MWCNT hybrid nanofluid past an exponential shrinkable permeable sheet with significant influence of slip and chemical reaction. More about the significance of nanofluid can be further seen in Refs. [17–19].

The recent discovery of hybrid nanofluid has piqued the interest of several researchers, prompting them to expand their numerical and experimental work. A binary hybrid nanofluid is a fluid that contains two distinct nanoparticles. It has already been established that the heat flow of hybrid nanofluid is far more impactful than the heat flow of regular nanoliquid or any other practicable fluid. The hybrid nanofluids have been utilized in different processes such as cooling of electronic equipment, welding, lubrication, thermal management of the vehicle, production of biomedicine and papers, and production of hydro-electric, making of space device and several other subject areas for a superior response concerning thermal conductivity than any regular nanofluids. Momin [20] analyzed experimentally the impact of mixed convection flow induced by a hybrid nanofluid. Takabi and Salehi [21] addressed the stream analysis through hybrid nanofluids within a sinusoidal enclosure. Sundar et al. [22] investigated on making of hybrid nanofluids and heat transmission. The thermal properties and friction factor were also depicted in this work. Nabil et al. [23] and Leong et al. [24] discovered the thermal characteristics of hybrid nanofluids. Das [25] demonstrates the mechanism and result of conventional as well as hybrid nanofluids. He noted that hybrid nanofluids have superior thermal efficiency, but that the choice of small particles is critical to making the liquid reliable. Hayat and Nadeem [26] reported an increase in heat transport provided by water-based Ag–CuO nanoparticles. The impact of Hall current on fluid flow past a revolving disc induced by hybrid nanofluid with magnetic and radiation effects was inspected by Acharya et al. [27]. They utilized the titanium and copper nanoparticles in their examination. Khan et al. [28] examined the hybrid nanofluid flow past a plate with aligned magnetic and non-Fourier heat flux effects. They observed that the velocity shrinkages and temperature uplifts due to hybrid nanoparticles. Recently, Maitra et al. [29] analyzed the performance of hydrothermal in a porous wavy cavity induced by hybrid nanofluid along with magnetic effect. They observed that the heat transfer can be controlled by adjusting the effective wavy wall length.

The utilization of nanofluid via a porous medium is an efficient scheme for improving convective heat transfer features in different processes in industries. As a result, researchers have paid close attention to the porous media approach. This is due to the fact that many industrial problems and especially in engineering applications, for example, groundwater, filtration of oil flow, thermal insulation, and all kinds of heat exchangers, this type of structure are observed. Das et. [30] observed that the mingling of high-energy and low-energy fluids has a significant impact on the performance of these devices. The influences of buoyancy flow past a vertical sheet in a porous medium were inspected by Merkin [31] and discovered that the occurrence of double solutions arises in the case of buoyancy opposing flow. Maghsoudi et al. [32] presented the analytic solution of free convective flow along with heat transfer induced by a non-Newtonian fluid saturated in a porous medium with the heat source. They observed that the velocity of fluid declines due to porosity; however, the temperature is unchanged. Further, Ahmed and Pop [33] and Roşca et al. [34] extended the work of Merkin [31] by considering nanofluid flow. Since then several researchers investigated the nanofluid flow in porous media by considering the different aspects (see Refs. [35–39]). Recently, Panigrahi et al. [40] examined the chemical reaction effect on the magneto flow of Casson fluid via a porous media through a stretchable sheet with nanofluid and Newtonian heating. Mahanthesh et al. [41] analyzed the dynamics of Darcy-Forchheimer flow of a Casson fluid through a circular tube with Joule heating and viscous dissipation.

Based on the preceding research, it is clear that, to the best knowledge of the authors, no attempts have been made thus far to investigate mixed convective hybrid nanofluid and heat transport with nonlinear heat source/sink through a cylinder in porous media with subject to radiation effects. Moreover, in light of various real-world problems, another factor that influences heat transfer is the heat source/sink. The distribution of heat in the entire domain can be changed when the heat source/sink is initiated. Basha et al. [42], Elgazery [43], Makinde et al. [44], and Gireesha [45] handled more interesting discussions on the impact of nonlinear heat source/sink. Therefore, the purpose of the present exploration is to examine the hybrid nanofluid flow along with a vertical permeable cylinder in porous media with radiative mixed convection. Similarity renovation is used to frame leading equations, which are then illustrated using the bvp4c technique. We believe that the current results can be utilized in real-world applications in the different fields of thermal engineering, cooling and heating systems, energy production, enzymes, etc.

2. Mathematical modeling of the problem

2.1. The description of governing equations with boundary conditions (BCs)

We consider the steady two-dimensional axisymmetric radiative flow of water-based Cu–Al$_2$O$_3$ hybrid nanofluid along with mixed convection through a porous vertical cylinder of radius r_0 saturated in a porous medium with a nonlinear heat source/sink. The radiative heat flux term was provoked in the requisite energy equation and is symbolically indicated by q_{rad}. The physical behavior of the dignified problem is modeled with the help of cylindrical coordinates as schematically revealed in Fig. 1, where $x-$ axis coordinate is reserved along the axial direction of the cylinder and $r-$ axis coordinate is considered normal to it. The assumed mainstream velocity is $U(x)$ in fluid at constant free-stream temperature T_∞, the wall variable temperature $T_w(x)$, and the axially symmetric mass transfer velocity v_w. Moreover, the hybrid nanoliquid is prepared by the mixture of two dissimilar types of nanoparticle such as copper (Cu) and aluminum oxide (Al$_2$O$_3$) composed with regular (viscous) fluid (H$_2$O). The thermophysical properties of the hybrid nanoparticles and the regular base fluid are taken to be in equilibrium. Therefore, here we employ the usual boundary layer approximations or scaling by which the constitutive steady basic leading equations, namely the standard continuity equation, the equation of Darcy by exercising Boussinesq approximation, and the equation of energy are expressed in the following form (see Bassom and Rees [46], Nield and Bajan [47])

$$\frac{\partial}{\partial x}(u\ r) + \frac{\partial}{\partial r}(v\ r) = 0, \tag{1}$$

$$u = U(x) + \frac{g\beta_{Hbnf}K}{v_{Hbnf}}(T - T_\infty), \tag{2}$$

$$(\rho c_p)_{Hbnf}\left(u\frac{\partial T}{\partial x} + v\frac{\partial T}{\partial r}\right) = k_{Hbnf}\left(\frac{\partial^2 T}{\partial r^2} + \frac{1}{r}\frac{\partial T}{\partial r}\right) - \frac{1}{r}\frac{\partial}{\partial r}(rq_{rad}) + Q'''. \tag{3}$$

In the aforementioned equations, v and u are the components of velocity in the respective coordinates of $r-$ and $x-$ axes while these coordinates, further considered the requisite distance to the surface of cylinder and perpendicular to it, respectively. However, T the temperature of the fluid, K the permeability of the porous medium, and g the acceleration due to gravity while the other symbols demonstrate the hybrid nanoparticles which are demarcated later in the individual section.

Additionally, the last term Q''' in the right-hand side of equation (3) illustrates the role of non-uniform or irregular heat source, which can be demonstrated as [see Refs. [48,49]]:

$$Q''' = \frac{k_{Hbnf}U(x)}{xv_{Hbnf}}\left[A^*(T_w - T_\infty)e^{-\xi} + B^*(T - T_\infty)\right], \tag{4}$$

where the exponentially decaying space coefficients and the temperature-dependent heat sink/source are dignified by A^* and B^*, respectively. Therefore, the positive value of A^* and B^* corresponds to the phenomenon of heat source while the negative value of A^*
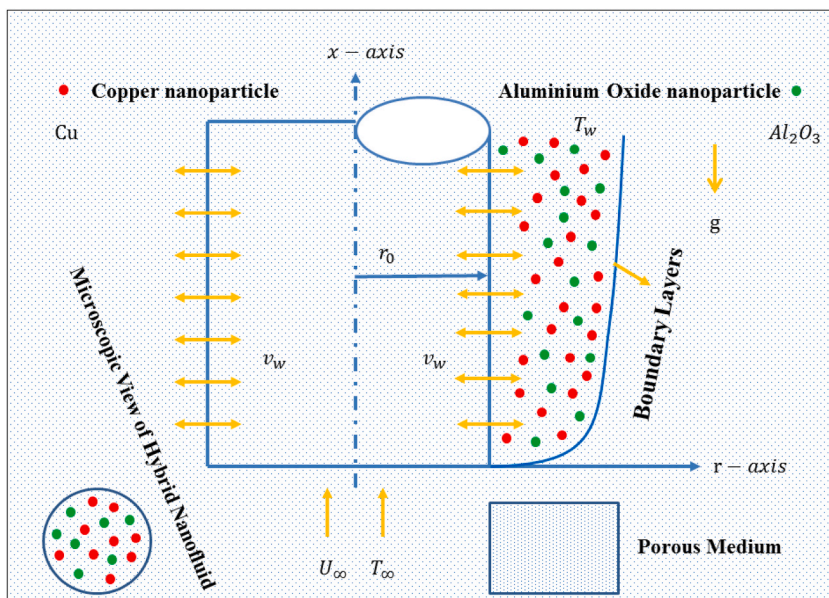
Fig. 1. Physical model of the flow problem embedded hybrid nanofluids.

and B^* corresponds to the phenomenon of the heat sink. Besides, the second last term on the right-hand side of equation (3) namely called the radiative heat flux q_{rad} which is demarcated via the Rosseland approximation as follows [2]:

$$q_{rad} = -\frac{4\sigma_d}{3k_d}\left(\frac{\partial T^4}{\partial r}\right), \tag{5}$$

where σ_d and k_d exemplify the Stefan Boltzmann constant and the mean absorption coefficient, respectively. Now executing the special Taylor series to expand the fourth power of T^4 around a unique point T_∞ and ignoring the higher-order power, one obtains the form as:

$$T^4 \cong 4TT_\infty^3 - 3T_\infty^4. \tag{6}$$

For the present model the following subject to physical boundary conditions (BCs) are employed as follows:

$$\begin{cases} v = v_w, \ T = T_w(x) \ \text{ at } \ r = r_0, \\ u \to U(x), T \to T_\infty \text{ as } \ r \to \infty, \end{cases} \tag{7}$$

where, v_w is the mass transfer velocity with $v_w = 0$ for the impermeable surface, $v_w > 0$ for suction, and $v_w < 0$ for blowing or injection, respectively. Furthermore, the surface temperature and ambient velocity of the cylinder as a variable function are denoted by $T_w(x)$ and $U(x)$, respectively, which are mathematically expressed as (see Mahmood and Merkin [50]):

$$T_w(x) = T_\infty + \frac{x \ \Delta T}{L} \text{ and } U(x) = \frac{xU_\infty}{L}, \tag{8}$$

where the length of characteristics and difference temperature is dignified by L and ΔT, respectively.

2.2. Model and the thermophysical features of the hybrid nanofluids

This section of the work highlights the significant expression and the detailed description of the considered water-based Cu–Al$_2$O$_3$ hybrid nanofluid model. This given model is made of two distinct nanoparticles such as copper (Cu) and aluminum oxide (Al$_2$O$_3$) into the ordinary base fluid (H$_2$O). About these available published work such as Hayat et al. [51] and Khan et al. [52] by which they have confined the upcoming basic steady governing equations along with the implemented suitable properties of the hybrid nanofluid which attained the vital flow dynamics accurately. The mathematical expressions for the described water-based Cu–Al$_2$O$_3$ hybrid nanofluid model are illustrated in Table 1.

Further, the thermophysical properties of the base fluid along with the copper (Cu) and aluminum oxide (Al$_2$O$_3$) nanoparticles are demarcated in Table 2.

Where the subscripts *Hbnf*, *nf* and *f* stand for the hybrid nanofluid, nanofluid, and base or regular fluid, respectively, while the other mathematical symbols like $k_f, \mu_f, (\rho c_p)_f, \beta_f$ and ρ_f designate the thermal conductivity, viscosity, heat capacity, thermal expansion coefficient, and the respective density of the viscous fluid. Also, for the simplicity in whole computations of the literature, the symbols or notations such as φ_1 and φ_2 represented the solid volume fraction of nanoparticles for the copper (Cu) and aluminum oxide (Al$_2$O$_3$) nanoparticles, respectively.

2.3. Similarity transformation

To ease the analysis of the considered problem, we here introduce the following similarity variables which can take place as:

$$\psi = \frac{2v_f x}{\varepsilon}F(\eta), T = T_\infty + \frac{x\Delta T}{L}\theta(\eta), \xi = \frac{r^2 - r_0^2}{r_0^2 \varepsilon}, \tag{9}$$

where $\varepsilon = \frac{2}{r_0}\sqrt{\frac{v_f L}{U_\infty}}$ is the curvature parameter, v_f is the kinematic viscosity, and ψ is the stream function which is defined in the following usual way $u = \frac{1}{r}\frac{\partial \psi}{\partial r}$ and $v = \frac{1}{r}\frac{\partial \psi}{\partial x}$.

Table 1
Thermophysical characteristics of the water-based Cu–Al$_2$O$_3$ hybrid nanofluid [53].

Properties	Hybrid nanofluid
Absolute viscosity	$\mu_{Hbnf}/\mu_f = 1/(1 - \varphi_{Cu} - \varphi_{Al_2O_3})^{2.5}$
Thermal conductivity	$k_{Hbnf}/k_f = (A_a + A_b)/(A_a + A_c),$
	where $A_a = \dfrac{(\varphi_{Cu}k_{Cu} + \varphi_{Al_2O_3}k_{Al_2O_3})}{\varphi_{Cu} + \varphi_{Al_2O_3}},$
	$\begin{cases} A_b = 2k_f + 2(\varphi_{Cu}k_{Cu} + \varphi_{Al_2O_3}k_{Al_2O_3}) - 2(\varphi_{Cu} + \varphi_{Al_2O_3})k_f, \\ A_c = 2k_f - (\varphi_{Cu}k_{Cu} + \varphi_{Al_2O_3}k_{Al_2O_3}) + (\varphi_{Cu} + \varphi_{Al_2O_3})k_f, \end{cases}$
Heat capacity	$(\rho c_p)_{Hbnf}/(\rho c_p)_f = \begin{cases} \varphi_{Cu}((\rho c_p)_{Cu}/(\rho c_p)_f) + \varphi_{Al_2O_3}((\rho c_p)_{Al_2O_3}/(\rho c_p)_f) + \\ (1 - \varphi_{Cu} - \varphi_{Al_2O_3}) \end{cases}$
Thermal expansion	$(\rho\beta)_{Hbnf}/(\rho\beta)_f = \begin{cases} \varphi_{Cu}((\rho\beta)_{Cu}/(\rho\beta)_f) + \varphi_{Al_2O_3}((\rho\beta)_{Al_2O_3}/(\rho\beta)_f) + \\ (1 - \varphi_{Cu} - \varphi_{Al_2O_3}) \end{cases}$
Density	$\rho_{Hbnf}/\rho_f = \{\varphi_{Cu}(\rho_{Cu}/\rho_f) + \varphi_{Al_2O_3}(\rho_{Al_2O_3}/\rho_f) + (1 - \varphi_{Cu} - \varphi_{Al_2O_3})$

Table 2

Thermophysical properties of the nanoparticles and base fluid [54,55].

Physical properties	Water	Al_2O_3	Cu
$k(W/mK)$	0.613	40	401
$c_p(J/kgK)$	4179	765	385
$\beta \times 10^{-5}(K)^{-1}$	21.00	0.85	1.65
$\rho(kg/m^3)$	997.1	3970	8933
Pr	6.2	–	–

Now utilizing equation (9) along with the choice of Eq. (8), equation (1) is identically satisfied while equations (2) and (3) and the BCs (7) are reduced to the subsequent dimensionless form of ODEs as:

$$F' = 1 + \lambda \frac{(\rho\beta)_{Hbnf}\big/(\rho\beta)_f}{\mu_{Hbnf}/\mu_f}\theta, \tag{10}$$

$$\left(\frac{k_{Hbnf}}{k_f} + \frac{4}{3}R_d\right)[(1+\varepsilon\xi)\theta'' + \varepsilon\theta'] + \frac{\left(\frac{k_{Hbnf}}{k_f}\right)\left(\frac{\rho_{Hbnf}}{\rho_f}\right)}{\frac{\mu_{Hbnf}}{\mu_f}}\left(A^* e^{-\xi} + B^*\theta\right)$$
$$+ \Pr\frac{(\rho c_p)_{Hbnf}}{(\rho c_p)_f}(F\theta' - \theta F') = 0, \tag{11}$$

along with the appropriate BCs are

$$F(0) = S, \theta(0) = 1, \theta(\infty) = 0. \tag{12}$$

In these dimensionless similarity equations, the involved influential parameters are namely demarcated as $Pe_L = \frac{LU_\infty}{\alpha_m}$ is the Peclet number, $R_d = \frac{4\sigma_d T_\infty^3}{k_d k_f}$ is the radiation parameter, $Ra_L = \frac{g\beta_f K\Delta TL}{\alpha_m v_f}$ is the Rayleigh number, $\lambda = \frac{Ra_L}{Pe_L}$ is the buoyancy parameter (ratio of free to forced convection velocity scales), and $S = -\frac{v_w r_0 \varepsilon}{2v_f}$ is the constant mass flux parameter with $(S < 0)$ for blowing and $(S > 0)$ for suction. Meanwhile, the primes indicate the requisite differentiation with respect to the pseudo-similarity variable ξ. In addition, combining equations (10) and (11), we finally have the equation

$$A_1(1+\varepsilon\xi)F''' + A_1\varepsilon F'' + A_4(FF'' - F'2 + F') + \lambda A_2 A_3 A^* e^{-\xi} + A_2 B^*(F'-1) = 0. \tag{13}$$

In which:

$$A_1 = \left(\frac{k_{Hbnf}}{k_f} + \frac{4}{3}R_d\right), A_2 = \frac{\left(\frac{k_{Hbnf}}{k_f}\right)\left(\frac{\rho_{Hbnf}}{\rho_f}\right)}{\frac{\mu_{Hbnf}}{\mu_f}}, A_3 = \frac{(\rho\beta)_{Hbnf}\big/(\rho\beta)_f}{\mu_{Hbnf}/\mu_f}, A_4 = \frac{(\rho c_p)_{Hbnf}}{(\rho c_p)_f}\Pr.$$

Or

$$(1+\varepsilon\xi)F''' + \varepsilon F'' + \frac{(\rho c_p)_{Hbnf}\big/(\rho c_p)_f \Pr}{\left(\frac{k_{Hbnf}}{k_f} + \frac{4}{3}R_d\right)}(FF'' - F'2 + F') +$$
$$\frac{(k_{Hbnf}/k_f)(\rho_{Hbnf}/\rho_f)}{\left(\frac{k_{Hbnf}}{k_f} + \frac{4}{3}R_d\right)\frac{\mu_{Hbnf}}{\mu_f}}\left(\lambda\frac{(\rho\beta)_{Hbnf}\big/(\rho\beta)_f}{\mu_{Hbnf}/\mu_f}A^* e^{-\xi} + B^*(F'-1)\right) = 0. \tag{13a}$$

The subjected boundary conditions (BCs) are

$$F(0) = S, F'(0) = 1 + \lambda\frac{(\rho\beta)_{Hbnf}\big/(\rho\beta)_f}{\mu_{Hbnf}/\mu_f}, F'(\infty) = 1. \tag{14}$$

2.4. Skin friction coefficient

The important component of the engineering physical quantities or gradients is the skin friction coefficient C_F, which is demarcated as

$$C_F = \frac{2\tau_w}{\rho U_\infty U}, \tag{15}$$

where τ_w is the wall shear stress and is given by $\tau_w = \mu_{Hbnf} \frac{\partial u}{\partial r}\Big|_{r=r_0}$.

Utilizing the similarity variables (9) into equation (15), one obtains the following reduced form of the skin friction coefficient:

$$\frac{1}{2}\sqrt{Re_L}C_F = \frac{\mu_{Hbnf}}{\mu_f}F''(0) \tag{16}$$

where $Re_L = \frac{U_\infty L}{v_f}$ is the local Reynolds number.

3. Results and discussion

In this section, we have physically interpreted and geometrically discuss our dual nature outcomes in the complete form. Before going towards this, we have to first solve equation (13) or (13a) with the boundary condition (14) via a built-in function available in MATLAB by the usual numerical scheme namely as boundary value problem of the fourth-order (bvp4c). The considered numerical scheme is based on the finite difference method which is also known as the 3-Stage Lobatto IIIA formula. Therefore, the complete procedure of the considered scheme is well documented by many researchers like Shampine et al. [56] and Khan et al. [55] which is not being repeated here. Moreover, to validate our numerical scheme or computational code, we have produced a graphical figure (see Fig. 2) for the first and second branch solutions to show the comparison for the limiting cases with the available information of Shu et al. [57]. The current outcomes of the velocity profile for the various values of S (without the influence of the nanoparticles volume fraction φ_1 and φ_2, the coefficients of the internal heat source/sink factor A^* and B^* and the radiation parameter) are compared graphically with the existing published results of Shu et al. [57] when $\lambda = -1$, $Pr = 1.0$ and $\varepsilon = 5.0$. The calculation output displays that the existing outcome of both dissimilar branches are in exceptional toning with the reported published outcomes, therefore, it gives us the confidence to find the unavailable results by the usually considered scheme. In addition, our main objectives are to assess the influences of the mixed convection parameter λ, mass transfer parameter S, radiation parameter R_d, volume fraction of nanoparticles φ_1 and φ_2, curvature parameter ε, and the coefficients of the internal heat source/sink factor A^* and B^* on dimensionless velocity and friction factor of the water-based Cu–Al$_2$O$_3$ hybrid nanofluid for the first and second solution branches are illustrated in Figs. 3–10. For the whole simulations, we have fixed and defined the following finite range of influential parameters such as: $0 \leq R_d \leq 1.0$, $-5 \leq \lambda \leq 5$, $3 \leq \varepsilon \leq 10$, $-3 \leq A^* \leq 3$, $-3 \leq B^* \leq 3$, $-5 \leq S \leq 5$ and $\varphi_1, \varphi_2 = 0.03$. The computational values of the skin friction coefficient for the first branch and second branch solutions owing to the impact of sundry parameters are highlighted in Table 3. The results explore that the fluid wall drag force are enhanced and declined due to influence of the curvature and radiation parameters, respectively. Therefore, the surface of the cylinder will be more drag affected because of curvature and less drag affected due to radiation parameter. In addition, the friction factor uplifts in the situation of the heat source while the effect of the heat sink on the friction factor behaves in a reverse trend. The considered model has two dissimilar branch solutions. The first branch solution is physically stable and their curves are represented by the solid red and green lines while the second branch solution is not physically
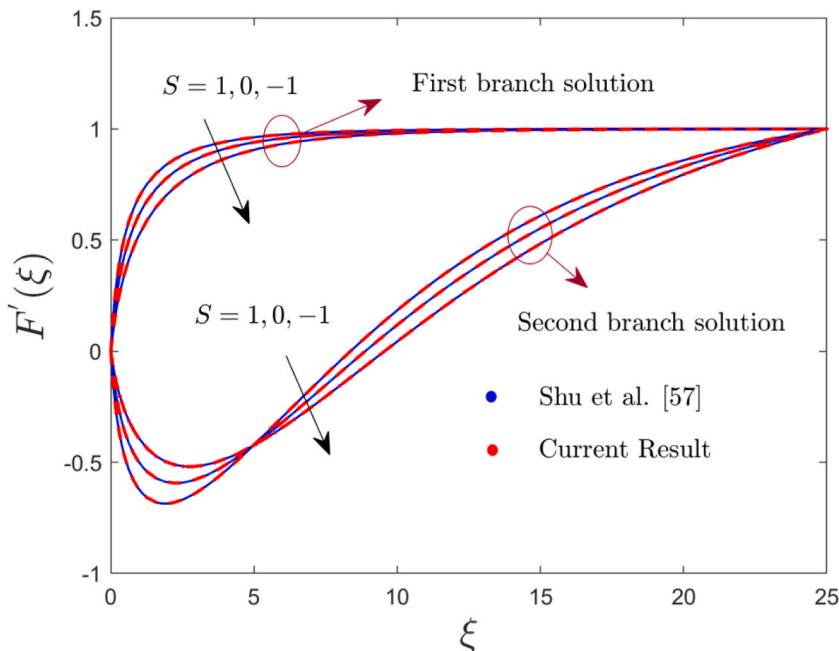
Fig. 2. Comparison of the velocity profiles $F'(\xi)$ for the several values of S with the available work of Shu et al. [57].
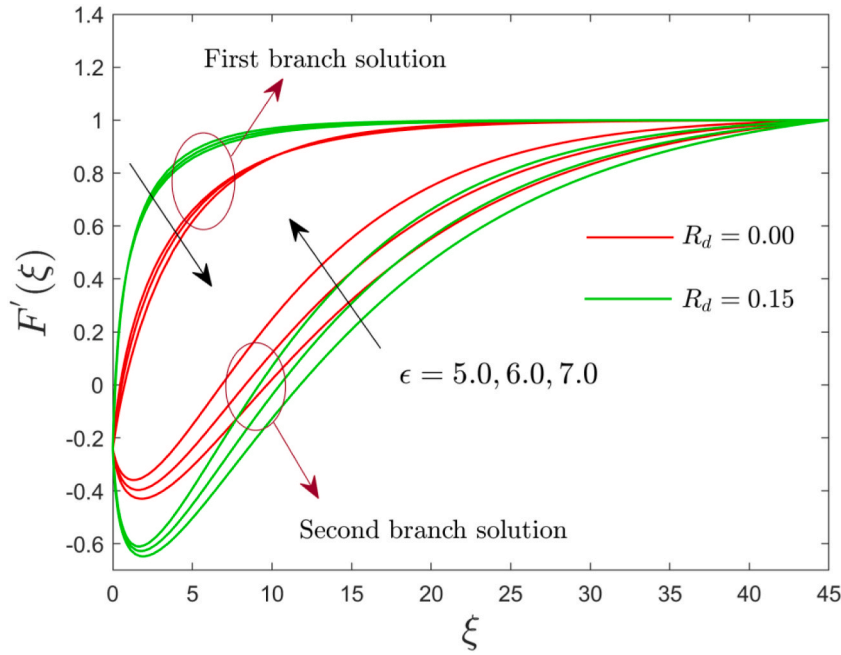
Fig. 3. Impact of ε on $F'(\xi)$.

Table 3

Numerical values of the reduced skin friction coefficient for the various varying selected parameters when $\varphi_1, \varphi_2 = 0.030$.

R_d	ε	S	λ	A^*, B^*	First branch solution	Second branch solution
0.15	5.0	0.5	−1.5	0.05	2.4370978	−1.4213762
0.35					2.3117585	−1.3641674
0.55					2.2151843	−1.3397394
0.15	5.0	0.5	−1.5	0.05	2.4370978	−1.4213762
	6.0				2.6752758	−1.5802445
	7.0				2.9047386	−1.7562656
0.15	5.0	0.5	−1.5	0.05	2.4370978	−1.4213762
		1.0			2.6047387	−1.5818494
		1.5			3.1093908	−1.9371240
0.15	5.0	0.5	−2.0	0.05	2.7997004	−0.6186420
			−1.5		2.4370978	−1.4213762
			−1.0		1.7998481	−2.0459810
			0.0		0.0000003	−3.3564244
			1.0		−2.3030793	−5.2276070
			1.5		−3.9091666	−6.6889431
			2.0		−4.9939381	−7.6573488
0.15	5.0	0.5	−1.5	0.05	2.4370978	−1.4213762
				0.10	2.3268391	−1.3689878
				0.15	2.2102865	−1.3030372
				−0.05	2.6422135	−1.4852932
				−0.10	2.7384125	−1.4956787
				−0.15	2.8310187	−1.4900338

stable (unstable) and is also denoted by the similar red and green solid lines curves (see by Merkin [58] and Wilks and Bramley [59]). Both branch curves are differentiated from one another by the highlighted solid marked circle in all figures. Meanwhile, the small solid distinct color balls denote the bifurcation or critical points where the solution of the first branch meets with the outcome of the second branch.

3.1. Influence of the curvature parameter on velocity and skin friction coefficient

Figs. 3 and 4 illustrate the influence of ε on profile of velocity and the skin friction coefficient of the water-based Cu–Al$_2$O$_3$ hybrid nanofluid for the first and second solution branches, respectively. The results of both figures were calculated for the non-radiation parameter $R_d = 0.0$ and radiation parameter $R_d = 0.15$. For the outcomes of velocity curves, it is detected that the first branch solution for the case of non-radiation parameter $R_d = 0.0$ and radiation parameter $R_d = 0.15$ decreases with the larger value of ε while

the impact of ε is treated opposite for the second branch solution. In general, this declining behavior in the stable (first) branch solution has occurred because the curvature parameter has a direct relationship with the viscosity. Therefore, with increasing ε the viscosity is increased according to the old concept of physics and as a consequence, the curves of velocity are decreasing. Moreover, the thickness of the momentum boundary-layer (MBL) is also diminished due to the stronger impact of ε. The velocity curves for the non-radiation parameter $R_d = 0.0$ are less as compared to the influence of the radiation parameter $R_d = 0.15$. Conversely, the outcomes of skin friction coefficient are disclosed in Fig. 4 for the case of buoyancy opposing flow ($\lambda < 0$) which specify that the solution for the branch of first curves is higher while lower for the second branch solution due to the augmentation in the value of ε. This picture display that the double outcomes (first and second branch solutions) exist for equation (11) or (11a) with BCs (12) for all values of $0 > \lambda \geq \lambda_C$, where $0 > \lambda_C$ is the bifurcation value of $\lambda < 0$, and all the varying values of ε. The two dissimilar branches (first and second) meet with each other at a bifurcation point, where the BL outcomes further than this position are not possible to be found owing to the strong BLS from the surface. The combined equations of energy and Darcy should be tackled numerically for the case of $\lambda_C \leq \lambda < 0$. Moreover, the acquired critical values for the selected choice of ε are written mathematically in the graph (see Fig. 4) for the non-radiation parameter $R_d = 0.00$ and radiation parameter $R_d = 0.15$, where the magnitude of the bifurcation value upsurges with a higher value of ε. To test the graph more censoriously, the magnitude of the bifurcation value is higher for the phenomenon of $R_d = 0.15$ as compared to the value of $R_d = 0.00$. Therefore, the existence of the solutions domain and the reduced friction factor is continuously escalated due to the larger curvature parameter ε.

3.2. Effect of the radiation parameter on velocity and skin friction coefficient

The impacts of R_d on $F'(\xi)$, and $\frac{1}{2}(\text{Re}_L)^{\frac{1}{2}}C_F$ for the first branch and second branch solutions are graphically demonstrated in Figs. 5 and 6, respectively. The outcomes divulged in Fig. 5 recognized a reducing behavior for the first branch solution with improving the value of R_d while the influence of R_d is reversed in the range of $0 \leq \xi \leq 2$ for the second branch solution and then start the similar behavior like the first branch solution as we increase the range of ξ. The space between the curves of the second branch solution is more as compared to the branch of the first solution curves. Moreover, the decreasing behavior of the velocity curve takes place because of the stronger effects of nanoparticles volume fraction generate superfluous viscous forces which diminished the thickness of the MBL as well as the tendency of the curves for velocity. In contrast, the friction factor decelerates for the first branch solution in the range of $-1.5 \leq \lambda \leq 0$ but elevates for the same branch in the range of $\infty < \lambda < -1.5$ with higher value of R_d while it reduces for the second solution. In addition, the small solid blue balls denote the bifurcation points ($\lambda_C < 0$) where both solution branches meet. For the varying value of the radiation parameter, we have found the following critical values such as -2.1805, -2.2470, and -2.3085. However, the magnitude of the critical or bifurcation value $|\lambda_C|$ improves by taking the larger impacts of the radiation parameter R_d. In this regard, the BLS augments with the higher implementation of the radiation parameter R_d.

3.3. Influence of the mass transfer parameter on velocity and skin friction coefficient

Fig. 7 displays the velocity curves for the non-radiation parameter $R_d = 0.00$ and radiation parameter $R_d = 0.15$ of the water-based Cu–Al$_2$O$_3$ hybrid nanoliquid for the first and second branch solution against ξ, with the successive increasing value of S. Also, the
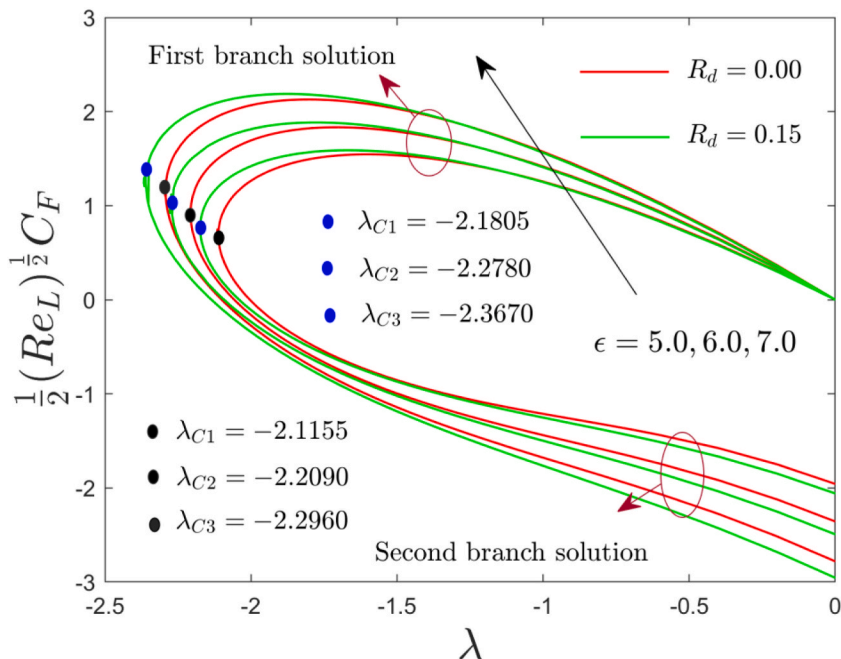
Fig. 4. Impact of ε on $\frac{1}{2}(\text{Re}_L)^{\frac{1}{2}}C_F$ versus λ.
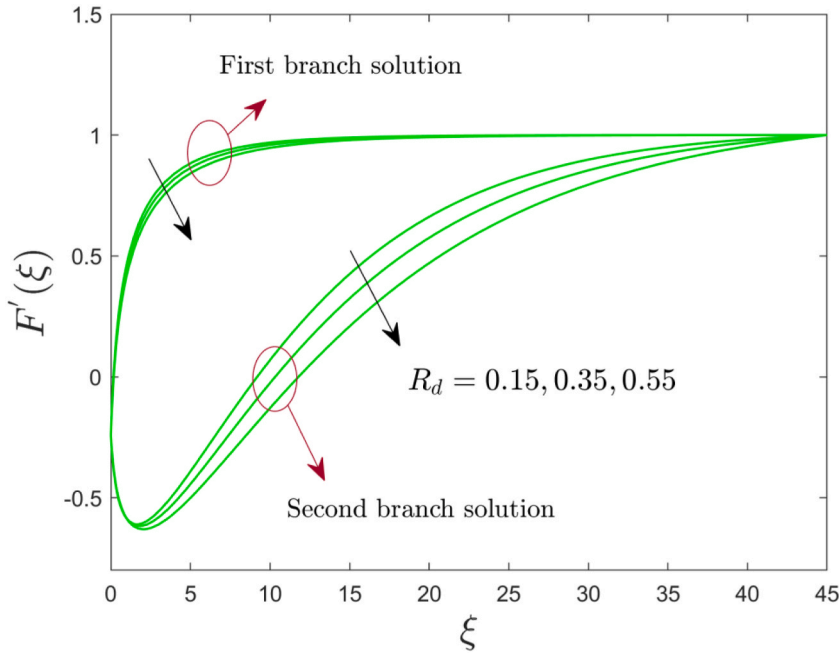
Fig. 5. Influence of radiation parameter R_d on $F'(\xi)$.
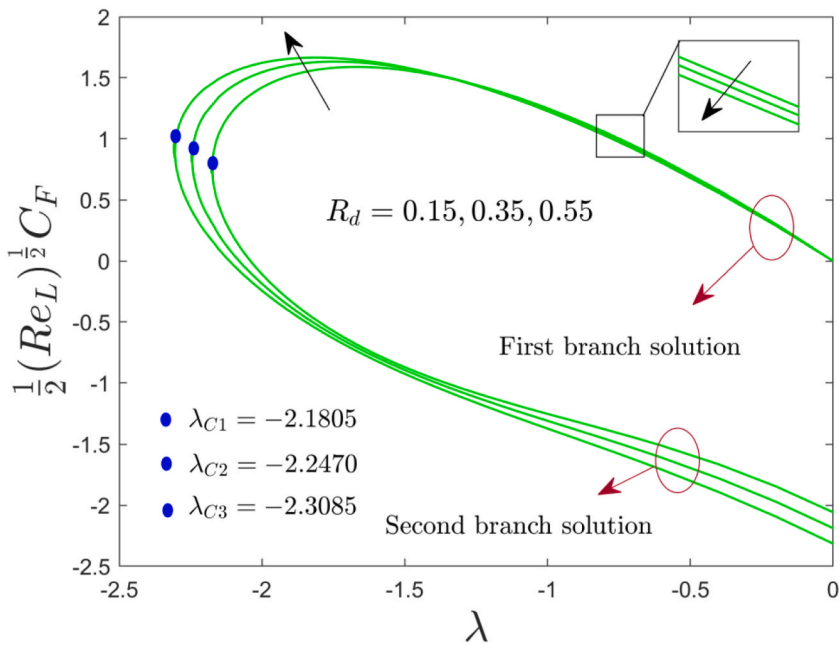
Fig. 6. Influence of radiation parameter R_d on $\frac{1}{2}(\mathrm{Re}_L)^{\frac{1}{2}}C_F$ versus λ.

considered picture disclosed that the BCs (12) at infinity are asymptotically converged. Meanwhile, this picture also recommends that the outcomes of the first branch solution increase owing to the larger value of S for the two distinct values of the radiation parameter, $R_d = 0.0$ and $R_d = 0.15$, while the impact of the S is completely changed for the lower (second) solution. For the first solution, the outcomes for the injection parameter are lower as compared to the suction parameter (see for both values of $R_d = 0.0$ and $R_d = 0.15$) while the curve middle of these two cases is for the impermeable surface $S = 0$. However, the comparison for the behavior of the curves is different like the first branch solution with the injection, suction, and impermeable value of the parameter S. In the physical point of view, the wall drag force reduces with the successive enhancing value of S, as an outcome, the velocity curves enrich. This enrichment of the velocity curves of the hybrid nanofluid generates reductions in the MBLT with significant improvement of S. Fig. 8 exemplifies
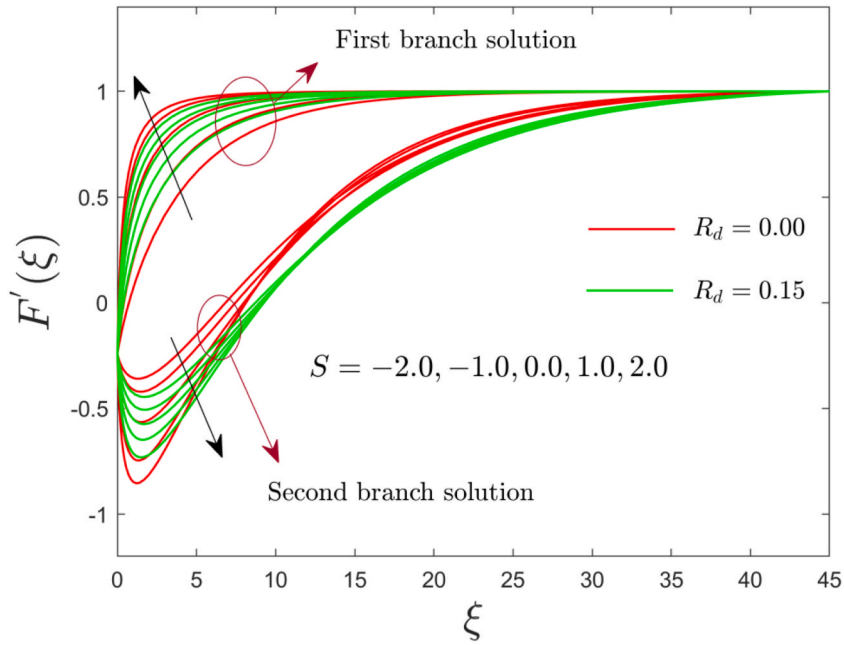
Fig. 7. Impact of S on $F'(\xi)$.

the impact of S on the friction factor for the non-radiation parameter $R_d = 0.0$ and radiation parameter $R_d = 0.15$ of the water-based Cu–Al$_2$O$_3$ hybrid nanofluid for both solution branches. Results here indicate that for the first solution branch, the friction factor upsurges while reduces for the second solution due to the continued superior value in S. In the considered picture the small solid ball of different colors signifies the bifurcation or critical point for change value of S. The magnitude of the critical point increase with a larger value of S and due to this pattern the separation of the boundary layer elevates. In addition, the magnitude of the critical value is higher for the value of $R_d = 0.15$ as compared to the value of $R_d = 0.0$. Also, noted from the picture that the wall drag force at the surface of the cylinder is more affected by the radiation parameter as relative to the non-radiation parameter.
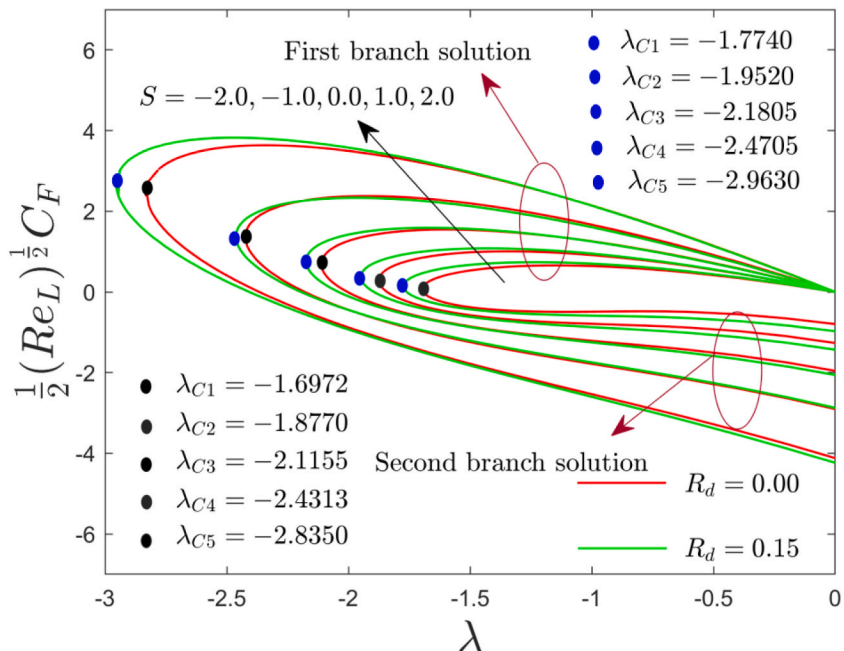
Fig. 8. Impact of S on $\frac{1}{2}(\mathrm{Re}_L)^{\frac{1}{2}} C_F$ versus λ.

3.4. Influence of the internal heat sink/source parameter on velocity profiles

Figs. 9 and 10 indicate the influence of A^* and B^* for the vertical cylinder (such as $R_d = 0.0$ and $R_d = 0.15$) on $F'(\xi)$. It can be observed that the dimensionless velocity profile of the water-based Cu–Al$_2$O$_3$ hybrid nanofluid decreases for the first branch solution with the internal heat source factor ($A^* > 0$ and $B^* > 0$) while it increases for the second branch solution (see Fig. 9). The curves in the first branch are lesser in magnitude for the selected value of the radiation parameter as paralleled to the non-radiation parameter. The presence of the heat source ultimately raises the fluid temperature by accumulating more heat to the system and reducing the thickness of the velocity boundary layer. On the other hand, the velocity curves enrich for the branch of the first solution owing to the internal heat sink parameter ($A^* < 0$ and $B^* < 0$) while the impact of the internal heat sink parameter ($A^* < 0$ and $B^* < 0$) is changed for the branch of the second solution. In this picture, the magnitude of $F'(\xi)$ curves is higher for the value of the radiation parameter in the first branch solution as compared to the absence of the thermal radiation in the energy equation. Physically, the internal heat sink which takes heat from the velocity boundary layer leads to the fall of the velocity boundary layer.

4. Conclusion

The problem of mixed convective axisymmetric flow conveying hybrid nanofluid through a cooled vertical permeable cylinder in a presence of porous medium subject to Darcy, irregular heat source/sink, and radiation effect is investigated. We use particular procedures for the exterior flow and variable surface cylinder temperature fluctuation that allows the set of PDEs to be transmuted the required ordinary (similarity) differential equations (Eq. (13) or 13a, 14). In addition, we have considered the impacts of the various involved distinguished parameters on velocity curves and reduced form of friction factor. Therefore, the final key remarks of the considered issue are following:

- A bifurcation value $\lambda_C < 0$ of the buoyancy factor for the case of buoyancy opposing flow ($\lambda < 0$) with solution possible only for the range of $\lambda_C \leq \lambda \leq 0$. However, the outcomes of the considered problem were impossible to find for the case of $\lambda \leq \lambda_C < 0$.
- The velocity curves shrinkages in both values of R_d (0.0 and 0.15) for the branch of upper solution (first) with the higher value of ε, while the influence of ε is dissimilar for the branch of lower (second) outcomes.
- The curves of velocity upsurge and decline for the first branch solution due to the enrichment in the value of S and radiation parameter R_d, respectively. Meanwhile, the velocity significantly shrinks for the second branch solution with a higher impact of S and radiation parameter R_d.
- The reduced form of the skin friction coefficient for the value of the radiation parameter $R_d = 0.15$ and non-radiation parameter $R_d = 0.0$ elevates for the branch of the first solution while decays for the second branch solution owing to the successive larger value of S and ε.
- The magnitude of the critical or bifurcation value for the values of $R_d = 0.15$ is more as compared to the choice of $R_d = 0.0$ with larger value of S and ε.
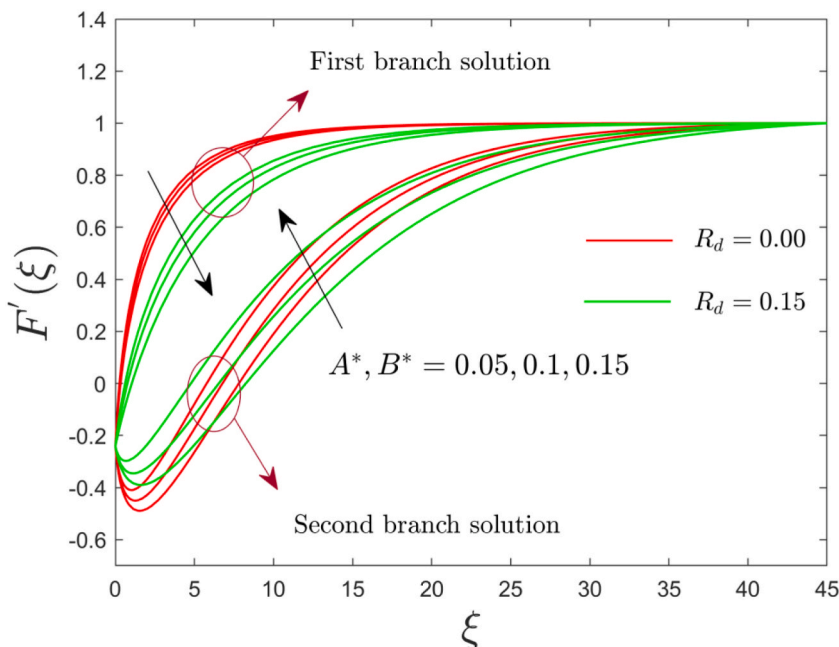
Fig. 9. Influence of A^* and B^* on $F'(\xi)$.
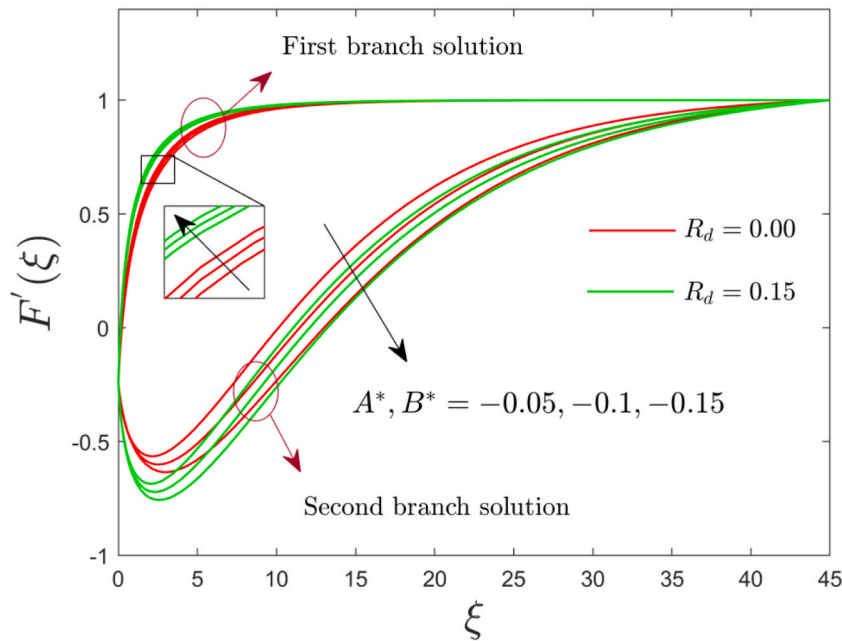
Fig. 10. Influence of A^* and B^* on $F'(\xi)$.

- For the branch of the first solution, the values of skin friction behave differently in the specific range of λ with radiation parameter while it is declined endlessly for the second branch solution as we move forward from positive to the negative side of the mixed convection parameter λ.

We hope that this work further can be extended to develop the heating system by utilizing the nanofluid.

Credit author statement

Umair Khan: Calculated analytically and performed computations in Matlab. Aurang Zaib designed mathematical model and writing. Anuar Ishak, Iaon Pop, **El-Sayed M. Sherif,** and **Yu-Ming Chu:** Provided significant feedback and assisted in the revised version of manuscript, **Iskandar Waini:** Validate the results. **Yu-Ming Chu:** Funding.

Declaration of competing interest

The authors declare that they have no known competing financial interests or personal relationships that could have appeared to influence the work reported in this paper.

Acknowledgment

References

[1] S.U.S. Choi, J.A. Eastman, Enhancing Thermal Conductivity of Fluids with Nanoparticles, in: Proceedings of the 1995 ASME International Mechanical Engineering Congress and Exposition, San Francisco, FED 231/MD 66, 1995, pp. 99–105.
[2] T. Hayat, S. Nadeem, A.U. Khan, Rotating flow of Ag-CuO/H$_2$O hybrid nanofluid with radiation and partial slip boundary effects, Europ. Phys. J. E 41 (6) (2018) 75.
[3] M. Khan, M.Y. Malik, T. Salahuddin, F. Khan, Generalized diffusion effects on Maxwell nanofluid stagnation point flow over a stretchable sheet with slip conditions and chemical reaction, J. Braz. Soc. Mech. Sci. Eng. 41 (2019) 178.
[4] G. Shahriari, P. Maghsoudi, S. Sadeghi, Impact of viscous dissipation on temperature distribution of a two-dimensional unsteady graphene oxide nanofluid flow between two moving parallel plates employing Akbari-Ganji method, Europ. J. Sust. Develop. Res. Europ. J. Sust. Develop. 2 (2) (2018) 24.
[5] P. Maghsoudi, G. Shahriari, H. Rasam, S. Sadeghi, Flow and natural convection heat transfer characteristics of non-Newtonian nanofluid flow bounded by two infinite vertical flat plates in presence of magnetic field and thermal radiation using Galerkin method, J. Cent. South Univ. 26 (2019) 1294–1305.
[6] H.H. Gorgani, P. Maghsoudi, S. Sadeghi, An innovative approach for study of thermal behavior of an unsteady nanofluid squeezing flow between two parallel plates utilizing artificial neural network, Europ. J. Sust. Develop. Res. 3 (1) (2019), em0069.
[7] E.M. Dede, Z. Yu, P. Schmalenberg, H. Iizuka, Thermal metamaterials for radiative plus conductive heat flow control, Appl. Phys. Lett. 116 (2020), 191902.
[8] Z. Xu, L. Li, X. Chang, Y. Zhao, W. Wang, Thermal field manipulation via a two-phase thermal metamaterial, Appl. Mater. Today 22 (2021), 100911.
[9] N.S. Elgazery, Nanofluids flow over a permeable unsteady stretching surface with non-uniform heat source/sink in the presence of inclined magnetic field, J. Egyptian Math. Soc. 27 (2019) 9.

[10] A. Zaib, U. Khan, I. Khan, El-S.M. Sherif, K.S. Nisar, A.S. Sheikh, Impact of nonlinear thermal radiation on the time-dependent flow of non-Newtonian nanoliquid over a permeable shrinking surface, Symmetry 12 (2020) 195.

[11] K. Ahmed, T. Akbar, Numerical investigation of magnetohydrodynamics Williamson nanofluid flow over an exponentially stretching surface, Adv. Mech. Eng. 13 (5) (2021) 1–12.

[12] H. Berrehal, G. Sowmya, O.D. Makinde, Shape effect of nanoparticles on MHD nanofluid flow over a stretching sheet in the presence of heat source/sink with entropy generation, Int. J. Numer. Methods Heat Fluid Flow (2021), https://doi.org/10.1108/HFF-03-2021-0225.

[13] D.A. Kashani, S. Dinarvand, Effects of dissolved solute on unsteady double-diffusive mixed convective flow of a Buongiorno's two-component nonhomogeneous nanofluid, Int. J. Numer. Methods Heat Fluid Flow 29 (1) (2019) 448–466.

[14] K. Swain, I.L. Animasaun, S.M. Ibrahim, Influence of exponential space-based heat source and Joule heating on nanofluid flow over an elongating/shrinking sheet with an inclined magnetic field, Int. J. Ambient Energy (2021), https://doi.org/10.1080/01430750.2021.1873854.

[15] K. Swain, B. Mahanthesh, Thermal enhancement of radiating magneto-nanoliquid with nanoparticles aggregation and Joule heating: a three-dimensional flow, Arabian J. Sci. Eng. 46 (2021) 5865–5873.

[16] K. Swain, F. Mebarek-Oudina, S.M. Abo-Dahab, Influence of MWCNT/Fe$_3$O$_4$ hybrid nanoparticles on an exponentially porous shrinking sheet with chemical reaction and slip boundary conditions, J. Therm. Anal. Calorim. (2021), https://doi.org/10.1007/s10973-020-10432-4.

[17] M. Senapati, S.K. Parida, K. Swain, S.M. Ibrahim, Analysis of variable magnetic field on chemically dissipative MHD boundary layer flow of Casson fluid over a nonlinearly stretching sheet with slip conditions, Int. J. Ambient Energy (2021) 1–15.

[18] P. Rana, B. Mahanthesh, K.S. Nisar, K. Swain, M. Devi, Boundary layer flow of magneto-nanomicropolar liquid over an exponentially elongated porous plate with Joule heating and viscous heating: a numerical study, Arabian J. Sci. Eng. 46 (2021) 12405–12415.

[19] K. Swain, S. Mishra, Flow and heat transfer analysis of water-based copper nanofluid over a nonlinearly stretching sheet: a numerical approach, Int. J. Ambient Energy (2021) 1–15.

[20] G.C. Momin, Experimental investigation of mixed convection with water-Al$_2$O$_3$ & hybrid nanofluid in inclined tube for laminar flow, Int. J. Sci. Technol. Res. 2 (2013) 195–202.

[21] B. Takabi, S. Salehi, Augmentation of the heat transfer performance of a sinusoidal corrugated enclosure by employing hybrid nanofluid, Adv. Mech. Eng. 6 (2014), 147059.

[22] L.S. Sundar, K.V. Sharma, M.K. Singh, A.C.M. Sousa, Hybrid nanofluids preparation, thermal properties, heat transfer and friction factor – a review, Renew. Sustain. Energy Rev. 68 (2017) 185–198.

[23] M.F. Nabil, W.H. Azmi, K.A. Hamid, N.N.M. Zawawi, G. Priyandoko, R. Mamat, Thermo-physical properties of hybrid nanofluids and hybrid lubricants: a comprehensive review on performance, Int. Commun. Heat Mass Tran. 8 (2017) 30–39.

[24] K.Y. Leong, K.Z.K. Ahmad, H.C. Ong, M.J. Ghazali, A. Baharum, Synthesis and thermal conductivity characteristics of hybrid nano fluids, Renew. Sustain. Energy Rev. 75 (2017) 868–878.

[25] P.K. Das, A review based on effect and mechanism of thermal conductivity of normal nanofluids and hybrid nanofluids, J. Mol. Liq. 240 (2017) 420–446.

[26] T. Hayat, S. Nadeem, Heat transfer enhancement with Ag–CuO/water hybrid nanofluid, Results Phys. 7 (2017) 2317–2324.

[27] N. Acharya, R. Bag, P.K. Kundu, Influence of Hall current on radiative nanofluid flow over a spinning disk: a hybrid approach, Phys. E Low-dimens. Syst. Nanostruct. 111 (2019) 103–112.

[28] U. Khan, A. Zaib, A. Ishak, S.A. Bakar, Time-dependent Blasius–Rayleigh–Stokes flow conveying hybrid nanofluid and heat transfer induced by non-Fourier heat flux and transitive magnetic field, Case Stud. Therm. Eng. 26 (2021), 101151.

[29] S. Maitra, D.K. Mandal, N. Biswas, A. Datta, N.K. Manna, Hydrothermal performance of hybrid nanofluid in a complex wavy porous cavity imposing a magnetic field, Mater. Today Proc. (2021), https://doi.org/10.1016/j.matpr.2021.09.078.

[30] S.K. Das, S.U.S. Choi, W. Yu, T. Pradeep, Nanofluids: Science and Technology, Wiley-Interscience, New Jersey, 2007.

[31] J.H. Merkin, Mixed convection boundary layer flow on a vertical surface in a saturated porous medium, J. Eng. Math. 14 (1980) 301–313.

[32] P. Maghsoudi, G. Shahriari, M. Mirzaei, M. Mirzaei, Natural convection of third-grade non-Newtonian fluid flow in a porous medium with heat source: analytical solution, Eur. Phys. J. Plus 133 (2018) 502.

[33] S. Ahmad, I. Pop, Mixed convection boundary layer flow from a vertical flat plate embedded in a porous medium filled with nanofluids, Int. Commun. Heat Mass Tran. 37 (2010) 987–991.

[34] N.C. Roşca, A.V. Roşca, T. Groşan, I. Pop, Mixed convection boundary layer flow past a vertical flat plate embedded in a non-Darcy porous medium saturated by a nanofluid, Int. J. Numer. Methods Heat Fluid Flow 24 (2014) 970–987.

[35] R.A. Mahdi, H.A. Mohammed, K.M. Munisamy, N.H. Saeid, Review of convection heat transfer and fluid flow in porous media with nanofluid, Renew. Sustain. Energy Rev. 41 (2015) 715–734.

[36] A. Kasaeian, R. Daneshazarian, O. Mahian, L. Kolsi, A.J. Chamkha, S. Wongwises, I. Pop, Nanofluid flow and heat transfer in porous media : a review of the latest developments, Int. J. Heat Mass Tran. 107 (2017) 778–791.

[37] Y. Menni, A.J. Chamkha, A. Azzi, Nanofluid transport in porous media: a review, Spec. Top Rev. Porous Media Int. J. 9 (2018) 1–16.

[38] K. Khanafer, K. Vafai, Applications of nanofluids in porous medium a critical review, J. Therm. Anal. Calorim. 135 (2019) 1479–1492.

[39] P. Maghsoudi, M. Siavashi, Application of nanofluid and optimization of pore size arrangement of heterogeneous porous media to enhance mixed convection inside a two-sided lid-driven cavity, J. Therm. Anal. Calorim. 135 (2019) 947–961.

[40] L. Panigrahi, J. Panda, K. Swain, G.C. Dash, Heat and mass transfer of MHD Casson nanofluid flow through a porous medium past a stretching sheet with Newtonian heating and chemical reaction, Karbala Int. J. Modern Sci. 6 (2020) 322–331.

[41] B. Mahanthesh, W. Al-Kouz, K. Swain, P.K. Rout, Computational modeling of heat transfer in magneto-non-Newtonian material in a circular tube with viscous and Joule heating, Heat Trans. 50 (2021) 6703–6718.

[42] H.T. Basha, R. Sivaraj, I.L. Animasaun, O.D. Makinde, Influence of non-uniform heat source/sink on unsteady chemically reacting nanofluid flow over a cone and plate, Defect Diffusion Forum 389 (2018) 50–59.

[43] N.S. Elgazery, Nanofluids flow over a permeable unsteady stretching surface with non-uniform heat source/sink in the presence of inclined magnetic field, J. Egyptian Math. Soc. 27 (9) (2019) 1–26.

[44] O.D. Makinde, F. Mabood, S.M. Ibrahim, Chemically reacting on MHD boundary-layer flow of nanofluids over a non-linear stretching sheet with heat source/sink and thermal radiation, Therm. Sci. 22 (1B) (2018) 495–506.

[45] B.J. Gireesha, R.S.R. Gorla, M.R. Krishnamurthy, B.C. Prasannakumara, Biot number effect on MHD flow and heat transfer of nanofluid with suspended dust particles in the presence of nonlinear thermal radiation and non-uniform heat source/sink, Acta Commentationes Univ. Tartuensis Math. 22 (1) (2018) 91–114.

[46] A.P. Bassom, D.A.S. Rees, Free convection from a heated vertical cylinder embedded in a fluid-saturated porous medium, Acta Mech. 116 (1996) 139–151.

[47] D.A. Neild, A. Bejan, Convection in Porous Media, fourth ed., Springer, New York, 2013.

[48] T. Hayat, S. Qayyum, A. Alsaedi, S. Asghar, Radiation effects on the mixed convection flow induced by an inclined stretching cylinder with non-uniform heat source/sink, PLoS One 12 (2017), e0175584.

[49] C.S. Sravanthi, Slip flow of nano fluid over a stretching vertical cylinder in the presence of non-linear thermal radiation and non-uniform heat source/sink, Sci. Iran. 25 (2018) 2098–2110.

[50] T. Mahmood, J.H. Merkin, Similarity solutions in axisymmetric mixed-convection boundary-layer flow, J. Eng. Math. 22 (1988) 73–92.

[51] T. Hayat, S. Nadeem, A.U. Khan, Rotating flow of Ag-CuO/H$_2$O hybrid nanofluid with radiation and partial slip boundary effects, Eur. Phys. J. E 41 (6) (2018) 1–9.

[52] U. Khan, I. Waini, A. Ishak, I. Pop, Unsteady hybrid nanofluid flow over a radially permeable shrinking/stretching surface, J. Mol. Liq. 331 (2021), 115752.

[53] U. Khan, A. Zaib, S. Abu Bakar, N.C. Roy, A. Ishak, Buoyancy effect on the stagnation point flow of a hybrid nanofluid toward a vertical plate in a saturated porous medium, Case Stud. Therm. Eng. 27 (2021), 101342.

[54] A.M. Rohni, S. Ahmad, I. Pop, Flow and heat transfer over an unsteady shrinking sheet with suction in nanofluids, Int. J. Heat Mass Tran. 55 (2012) 1888–1895.

[55] I. Waini, A. Ishak, I. Pop, Unsteady flow and heat transfer past a stretching/shrinking sheet in a hybrid nanofluid, Int. J. Heat Mass Tran. 136 (2019) 288–297.
[56] L.F. Shampine, S. Thompson, Solving DDEs in Matlab, Appl. Numer. Math. 37 (4) (2001) 441–458.
[57] J.J. Shu, Q.W. Wang, I. Pop, Dual solutions for opposing mixed convection in porous media, J. Heat Tran. 10 (2017) 139.
[58] J.H. Merkin, On dual solutions occurring in mixed convection in a porous medium, J. Eng. Math. 20 (1986) 171–179.
[59] G. Wilks, J.S. Bramley, Dual solutions in mixed convection, Proc. R. Soc. Edinb. Sect. A (Math. Phys. Sci.): Mathematics 87 (1981) 349–358.

Nomenclature

$U(x)$: Free-stream velocity (m/s)
K: The permeability of the porous medium
T: Temperature of the fluid (K)
v_w: Mass transfer velocity (m/s)
$T_w(x)$: Variable temperature at the wall surface of the cylinder (K)
T_∞: Constant Free-stream temperature (K)
q_{rad}: Thermal radiative heat flux
x, r, θ: Cylindrical coordinates (m)
u, v, w: Velocity components (m)
g: Acceleration due to gravity (m/s^2)
c_p: Specific heat at constant pressure (J/KgK)
A^*, B^*: Internal heat source/sink coefficients
k_d: Mean absorption coefficient
ΔT: Temperature difference (K)
L: Characteristic length of the cylinder (m)
U_∞: Constant ambient velocity (m/s)
F: Dimensionless stream function
Ra_L: Rayleigh number
Pe_L: Peclet number
S: Mass suction parameter
Pr: Prandtl number
R_d: Radiation parameter
τ_w: Shear stress at the wall surface of the cylinder
C_F: Coefficient of skin friction
k: Thermal conductivity
Re_L: Local Reynolds number

Greek symbols

σ_d: Stefan Boltzmann constant
ρ: Density
β: Thermal expansion coefficient
μ: Absolute viscosity
υ: Kinematic viscosity
ξ: similarity variable
ψ: Stream function
λ: Mixed convection or buoyancy parameter
θ: Dimensionless temperature
Q''': Irregular heat source/sink
ε: Curvature parameter

Acronyms

BCs: Boundary conditions
PDEs: Partial differential equations
ODEs: Ordinary differential equations
bvp4c: Boundary value problem of fourth-order
MBL: Momentum boundary layer

Subscripts

Al_2O_3: Aluminum dioxide nanoparticles
Cu: Copper nanoparticles
w: Condition at surface
nf: Nanofluid
Hbnf: Hybrid nanofluid
∞: Ambient condition
f: Base fluid

Superscript

$'$: Differentiation with respect to ξ